Accepted Manuscript

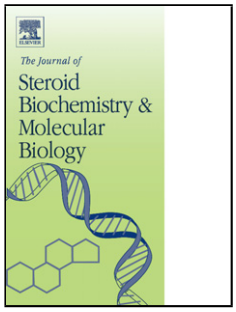

Title: Antineoplastic effect of $1\alpha,25(OH)_2D_3$ in spheroids from endothelial cells transformed by Kaposi's sarcoma-associated herpesvirus G protein coupled receptor

Authors: Alejandra Suares, Cinthya Tapia, Verónica González-Pardo

PII: S0960-0760(18)30508-9
DOI: https://doi.org/10.1016/j.jsbmb.2018.10.004
Reference: SBMB 5228

To appear in: *Journal of Steroid Biochemistry & Molecular Biology*

Received date: 25-8-2018
Revised date: 27-9-2018
Accepted date: 6-10-2018

Please cite this article as: Suares A, Tapia C, González-Pardo V, Antineoplastic effect of $1\alpha,25(OH)_2D_3$ in spheroids from endothelial cells transformed by Kaposi's sarcoma-associated herpesvirus G protein coupled receptor, *Journal of Steroid Biochemistry and Molecular Biology* (2018), https://doi.org/10.1016/j.jsbmb.2018.10.004

Antineoplastic effect of 1α,25(OH)$_2$D$_3$ in spheroids from endothelial cells transformed by Kaposi's sarcoma-associated herpesvirus G protein coupled receptor.

Alejandra Suares[#], Cinthya Tapia[#], Verónica González-Pardo[*]

Instituto de Ciencias Biológicas y Biomédicas del Sur (INBIOSUR), Departamento de Biología Bioquímica y Farmacia, Universidad Nacional del Sur (UNS)-CONICET, San Juan 670, (8000) Bahía Blanca, Argentina.

[#]These authors equally contributed to this work

[*]**Corresponding author:** Dr. Verónica González-Pardo, Departamento Biología Bioquímica & Farmacia, INBIOSUR, CONICET, Universidad Nacional del Sur. San Juan 670, 8000 Bahía Blanca- Argentina. Tel: +54-291-4595101, ext. 2430 .*Fax*: +54-291-4595130. *E-mail*: vgpardo@criba.edu.ar

Highlights

- vGPCR cells developed multicellular spheroids (MCS) in a non-adherent surface.
- vGPCR MCS size and architecture changed after 1α,25(OH)$_2$D$_3$ treatment.
- 1α,25(OH)$_2$D$_3$ reduced HIF-1α and increased BIM and P21expression in MCS.
- Akt and ERK1/2 phosphorylation was inhibited by 1α,25(OH)$_2$D$_3$ treatment in MCS.

Abstract

The Kaposi's sarcoma-associated herpesvirus G protein-coupled receptor (KSHV/vGPCR) is a key molecule in the pathogenesis of Kaposi's sarcoma. In endothelial cells, tumor maintenance and NF-κB activation depends on vGPCR constitutive expression and activity. We have previously demonstrated that $1\alpha,25(OH)_2D_3$ induces apoptosis in a VDR dependent manner, inhibits vGPCR cell growth and NF-κB activity. In this study, we developed a method to obtain multicellular spheroids (MCS) from endothelial cells expressing vGPCR in order to test whether MCS have a similar response to 2D-cultures after $1\alpha,25(OH)_2D_3$ treatment. Firstly, we found that vGPCR MCS started to form at 2^{nd} day-growth, reaching a diameter up to 300 μm at 7^{th} day-growth, whereas cells without vGPCR expression (SVEC) developed spheroids earlier and remained smaller throughout the period monitored. Secondly, vGPCR MCS size and architecture were analyzed during $1\alpha,25(OH)_2D_3$ (0.1-100 nM, 48 h) treatment. We found that once treated with 10 nM of $1\alpha,25(OH)_2D_3$ the initials MCS began a slight disaggregation with no changes in size; whereas at the higher dose (100 nM) the architecture of MCS was found completely broken. Furthermore, VDR mRNA expression increased significantly and this change was accompanied by a reduction of HIF-1α, an increase of VEGF, p21 and Bim mRNA expression. Finally, results from Western blot analysis showed that $1\alpha,25(OH)_2D_3$ decreased Akt and ERK1/2 protein phosphorylation. In conclusion, these data have revealed that $1\alpha,25(OH)_2D_3$ inhibits vGPCR MCS proliferation and induces apoptosis similar to vGPCR cells growing in 2D-cultures.

Keywords: multicellular spheroids, vGPCR, antineoplastic effects, active vitamin D

Abbreviations

MCS (multicellular spheroids), FBS (fetal bovine serum), HIF-1α (hypoxia-inducible factor 1α), KSHV/vGPCR (Kaposi's sarcoma-associated herpesvirus G protein-coupled receptor), MCS (multicellular spheroids), VDR (Vitamin D Nuclear Receptor) and VEGF (Vascular Endothelial Growth Factor).

1. Introduction

Viral cancers represent 12% of all human cancers and occur mostly in the developing world. Oncoviruses carry viral oncogenes that activate the same host signaling pathways, regulate growth and apoptosis as well as the development of non-viral cancers [1]. Kaposi's sarcoma (KS) is the most common cancer in HIV-infected untreated individuals and the infectious cause of this neoplasm is KS-associated Herpesvirus (KSHV or Human Herpesvirus 8) [2,3]. The viral G protein-coupled receptor (vGPCR) is the key molecule in this pathogenesis, and its transgenic expression induces angiogenic lesions similar to those observed in human KS lesions demonstrating strong angiogenic and tumoral effects [4]. The neovascular tumor conservation requires vGPCR continuous expression and activity in this type of cancer [5]. Recently, the reprogramming of lymphatic endothelial cells to mesenchymal cells, by KS vGPCR-iniciated, was studied in a three dimensional cell model. [6].

The most active form of vitamin D steroid hormone, 1α,25-Dihydroxyvitamin D_3 ($1\alpha,25(OH)_2D_3$ or calcitriol), performs a main role on intestinal calcium absorption and bone remodeling through its actions in intestine, bone, kidney and parathyroid gland [7]. Most of its actions depend on VDR, the vitamin D nuclear receptor, member of the nuclear receptor superfamily. Within the non-classical effects, data of antineoplastic activity on neoplastic cells in different types of cancer has been growing [8,9]. In recent years, it has been recognized that $1\alpha,25(OH)_2D_3$ exerts an anti-proliferative and pro-differentiating action in

many malignant cells and retards the development and growth of tumors in animal models [1,10,11]. 1α,25$(OH)_2D_3$ can inhibit angiogenesis, invasion and metastasis through the regulation of vascular endothelial growth factor (VEGF) [12,13] and the Wnt/β-catenin pathway in some types of tumors [8,14,15]. Likewise, 1α,25$(OH)_2D_3$ exhibits anti-inflammatory effects, including the suppression of the action of prostaglandins [8]. These actions provide basis for its potential use in cancer therapy and/or chemoprevention [16].

Many types of mammalian cells can aggregate and form multicellular spheroids (MCS) when cultured in suspension or a non-adhesive environment. The absence of cell-cell and cell–matrix interactions make monolayer cell cultures unable to reflect real tissues physiology and microenvironment [17]. Therefore, MCS have gained importance establishing an experimental *in vitro* model of intermediate complexity between monolayer cultures and tumors *in vivo* [18]. They can be developed from cellular monolayer cultures (2D cultures) or they can be derived from primary tumors [19]. Despite of presenting many of the limitations of an experimental model *in vitro*, MCS has opened up a new pathway for cytotoxic drug sensitivity tests, since cells adapt to the conditions imposed by the acquired spatial configuration [18]. Three-dimensional cell cultures can be develop by seeding the cells on artificial matrices. These matrices, act as a solid support for cells and are composed of hydrogels, fibers or beads that can be produced with different porosities and mechanical characteristics to mimic the extracellular tumoral matrix *in vivo* [20,21]. Xu and collaborators proposed the use of polymer structures for the development of multicellular spheroids of human prostate cancer (LNCaP) in a matrix of hyaluronic acid [22]. Matrices of alginates, collagen and agarose have been developed for the development of ovarian carcinoma spheroids (A2780), lymphoblasts (EL4) and epithelial cells (1308.1) [23]. We have previously demonstrated that 1α,25$(OH)_2D_3$ inhibits the growth of endothelial cells expressing vGPCR *in vitro* and *in vivo*, downregulates NF-κB pathway highly activated by

the viral receptor vGPCR and induces apoptosis in a VDR dependent manner [24–26]. In this work we developed a technique to obtain MCS from SVEC and vGPCR cells and tested whether vGPCR is required to MCS development and whether vGPCR MCS respond to $1\alpha,25(OH)_2D_3$ in a similar manner to vGPCR cells in 2D-cultures. This 3D culture of vGPCR cells would give us a better approach to elucidate the antineoplastic and anti-inflammatory mechanism of action of the active form of vitamin D in Kaposi's sarcoma.

2. Material and Methods

2.1. Chemicals and reagents

$1\alpha,25(OH)_2D_3$, and the antibiotic G418 were from Sigma-Aldrich (St. Louis, MO, USA). The antibodies used were rabbit monoclonal anti-P-ERK1/2 and anti-P-Akt (Cell Signaling Technology, Migliore Laclaustra, Buenos Aires, AR), anti-tubulin and anti-rabbit horseradish peroxidase–conjugated secondary antibody (Santa Cruz, CA, USA). Roche Applied Science (Indianapolis, IN, USA) provided high Pure RNA Isolation Kit. Immobilon P (polyvinylidene difluoride; PVDF) membranes were from Thermo Fisher; PCR primers for mouse GAPDH, vGPCR, VDR, HIF-1α, VEGF, A20, BIM and P21 were synthetized by Invitrogen (Thermo Fisher Scientific Inc., Rockford, IL, USA). For most applications, $1\alpha,25(OH)_2D_3$ was used at 10 nmol L^{-1} and 100 nmol L^{-1} since these concentrations show anti-proliferative effects in many tumor cell types.

2.2. Cell lines and transfections

As an experimental model of Kaposi's sarcoma, SV-40 immortalized murine endothelial cells that stably express vGPCR full length receptor (vGPCR), were utilized as we have previously described [27]. Stable overexpression of vGPCR promotes tumor formation in immune-suppressed mice and induces angiogenic lesions similar to those developed in Kaposi's sarcoma [5,28]. Transfected cells were selected with 500 μg mL^{-1} G418. Medium was freshly changed every other day.

2.3. Multicellular spheroids development

For qRT-PCR and micrographs studies, 96-well lipidure®-coat plates covered by a biocompatible polymer containing phosphocholine moiety were used (Amsbio, AMS Biotechnology, Europe). SVEC and vGPCR cells were seeded at 2,500 cell/well and cultured in DMEM with 10 and 5% FBS respectively. More restrictive growth conditions (decrease in serum) favor vGPCR expression. During $1\alpha,25(OH)_2D_3$ treatment, FBS was reduced to 2% due to the fact that the absence of serum triggers autophagy and apoptosis in these cells after prolonged incubation times. Therefore, this allows a better determination of the agonist mechanism of action [29]. For Western blot studies, common 24-multiwells covered with 3% agar were used. vGPCR cells were seeded at 12,000 cell/well and cultured in DMEM with 5% FBS. In both cases, spheroids development was followed through time.

2.4. Light field microscopy

Spheroids size and architecture from 3D culture were observed under a light field microscopy. Representative micrographs were captured by a Nikon TE300 Eclipse Inverted Microscope, equipped with a digital camera and objectives.

2.5. SDS-PAGE and Western blot

Whole MCS lysates were prepared as we have previously reported [25] and protein content was determined by the Bradford procedure [30]. Proteins were resolved (with SDS–PAGE) and transferred to PVDF membranes followed by Western blot analyzes that were effected as reported before [30]. Briefly, membranes were blocked and incubated with primary antibodies [anti- P-ERK1/2 (1:1000), anti-P-Akt (1:1000) or anti-Tubulin (1:1000)] diluted in TBST buffer (0.1% tween, 2.5% dry milk) overnight at 4°C. After three washes in TBST buffer, membranes were incubated with anti-rabbit (1:5000) horseradish peroxidase-conjugated secondary antibody 1h at room temperature. Later, after three washes in TBST buffer, blot signals were detected using an enhanced chemiluminescence kit according to the

manufacturer's instructions (Amersham ECL Western Blotting Detection Kit, GE Healthcare, Buenos Aires, AR). Images were scanned and quantified using ImageJ software, developed at the National Institutes of Health.

2.6. Quantitative real-time PCR

Total RNA for real-time quantitative reverse transcriptase polymerase chain reaction (qRT-PCR) analysis was isolated using the High Pure RNA Isolation Kit (Roche) as we have previously described [29]. Briefly, total RNA (0.5-1µg) was reverse transcribed using the kit High Capacity cDNA RT (Applied Biosystems, Thermofisher, Buenos Aires, AR) and qRT-PCR reactions were achieved on the resulting cDNA (5- 10 ng) in an ABI 7500 Real Time PCR system (Applied Biosystems, CA, USA) using specific primers. Primers sequences were as follows: *vGPCR:* (Fw) 5'-TGGTTCCCCTGATATACTCCTG-3' and (Rv) 5'-GGACATGAAAGACTGCCTGAG-3'; *murine VDR:* (Fw) 5'-AGGAGAGCACCCTTGGGCT-3' and (Rv) 5'-ACACACTCCACAGATCCGAGG-3' [25]; *murine HIF-1α:* (Fw) 5'-CGACACCATCATCTCTCTGG-3' and (Rv) 5'-AAAGGAGACATTGCCAGGTT-3';*murine VEGFa:* (Fw) 5'-ATGAACTTTCTGCTCTCTTGGGTG-3'and (Rv) 5'-GACTTCTGCTCTCCTTCTGTCGTG-3'; *murine GAPDH* (Fw) 5′-GAAGGTGAAGGTCGGAGTC-3′ and (Rv) 5′-GAAGATGGTGATGGGATTTC-3′ [31]; *murine A20:* (Fw) 5'-CATGAAGCAAGAAGAACGGAAGA-3' and (Rv) 5'-GAGGCCCGGGCACATT-3', *murine Bim:* (Fw) 5'-CGGTGGTGGAGGAACTCTTC-3'and (Rv) 5'-GCCCTCCCTTGTTTACATTCAC-3' [26]; *murine P21:* (Fw) 5'-TTGGAGTCAGGCGCAGATCCACA-3′ and (Rv) 5′-CGCCATGAGCGCATCGCAATC-3′ [32]. Reactions were carried out using the SYBR Green PCR Master Mix reagent (Applied biosystems, Thermofisher, Buenos Aires, AR). Gene expression was then analyzed by 2-delta delta Ct method using GAPDH as reference parameter [32].

2.7. Statistical analysis

Data are shown as means ± SD. Results from qRT-PCR and Western blot were analyzed by one way ANOVA followed by Bonferroni test. Different superscript letters indicate significant differences at $*p<0.05$.

3. Results

3.1. Development of MCS from SVEC and vGPCR cells

Based on the evidence mentioned in the introduction, we investigated whether endothelial cells (SVEC) or endothelial cells transformed by the expression of vGPCR (vGPCR) have the ability to develop MCS when are growing on a solid surface covered by a non-adherent polymer. For this, 96-well lipidure®-coat plates were used. SVEC and vGPCR cells were seeded at a density of 2,500 cell/well and cultured in DMEM with 10 and 5% FBS respectively and spheroids development was followed over time. **Fig. 1** shows MCS micrographs of SVEC and vGPCR cells obtained by light field microscopy from 1st day to 7th day-growth after seeding. It can be observed that both cell lines could form MCS, but the behavior of each cell line turned out to be different. In the case of SVEC cells, accelerated cellular aggregation was detected at 1st day-growth compared to vGPCR cells. However, they did not considerably increase their size, 50 μm approximately, within the following days. Whereas, vGPCR cells displayed a lower rate of aggregation at 1st day and bigger spheroids were observed at 2nd day-growth, reaching a diameter up to 300 μm, within 7th days-growth. The 5th day-growth was chosen to carry out the subsequent studies where the spheroids displayed a more uniform distribution.

3.2. MCS validation through vGPCR expression

It is well establish that stable expression of vGPCR is required for the development of cellular malignancy in Kaposi's sarcoma as was mentioned in the introduction [33]. Evidence support the fact that to elucidate the molecular mechanism of viral angiogenic oncogene

GPCR is essential to develop new therapies to the KSHV-induced malignancies [4,34]. In order to validate 3D cultures of SVEC and vGPCR cells, the expression of vGPCR and VDR genes was analyzed by qRT-PCR in spheroids developed from these cells lines at 5th day-growth (**Fig. 2**). As in 2D cultures, the expression of vGPCR mRNA was found greatly high in spheroids obtained from vGPCR cells in comparison with SVEC cells that lacks the viral receptor as expected (**Fig. 2A**). In addition, as was previously reported by our group in 2D cultures of vGPCR cells [27], VDR mRNA was significantly increased in vGPCR MCS compared to SVEC MCS (**Fig. 2B**).

3.3. 1α,25(OH)$_2$D$_3$ induces morphological changes and increases VDR expression in vGPCR MCS

To investigate the antiproliferative effect of 1α,25(OH)$_2$D$_3$ in vGPCR MCS, vGPCR spheroids at 5th day-growth were treated with increasing concentrations of 1α,25(OH)$_2$D$_3$ (0.1-100 nM) or vehicle (0.01% ethanol) during 48 hours. The morphology of the spheroids was evaluated by light field microscopy, and micrographs at the beginning and at the end of the treatment were captured (**Fig. 3A**). At the beginning of the treatment, zero time, control spheroids were observed compact with an average size in all conditions, which did not vary qualitatively at the time of completion of the experiment (48 h). 1α,25(OH)$_2$D$_3$, at 10 nM concentration, triggered changes in the structure of the spheroids. In general, cells adopted a slack arrangement and few spheroids disaggregated, whereas at the higher concentration (100 nM) the architecture of vGPCR MCS was found in most cases damaged; cells started to separate adopting a monolayer distribution; which resembles to the stage of spheroids formation. To evaluate the molecular response of these spheroids to 1α,25(OH)$_2$D$_3$ treatment, VDR mRNA was analyzed by qRT-PCR. As can be observed from **Fig. 3B,** VDR gene expression significantly increase after 1α,25(OH)$_2$D$_3$ treatment.

3.4. 1α,25(OH)$_2$D$_3$ exerts its antineoplastic effect through a mechanism that involves the inhibition of the pro-angiogenic factor HIF-1α

The initiation of angiogenesis is controlled by local hypoxia which induces the synthesis of pro-angiogenic factors that activate signaling pathways [35]. In response to local hypoxia the hypoxia-inducible factor 1α (HIF-1α) increases the expression of several pro-angiogenic factors including the vascular endothelial growth factor (VEGF) [36–38]. We studied whether 1α,25(OH)$_2$D$_3$ exerts its antineoplastic effects by inhibiting the expression of the pro-angiogenic factors HIF-1α and VEGF in vGPCR MCS. For this, the spheroids were treated with 1α,25(OH)$_2$D$_3$ (0.1-100 nM) or vehicle (0.01% ethanol) during 48 hours as mentioned before. Then, the expression of HIF-1α and VEGF mRNA was analyzed by qRT-PCR. As can be seen from **Fig. 4**, 1α,25(OH)$_2$D$_3$ significantly inhibited HIF-1α mRNA expression in a dose-dependent manner; on the contrary, VEGF mRNA expression significantly increased. There is existing data that 1α,25(OH)$_2$D$_3$ regulates VEGF production through vitamin D response elements in the VEGF promoter [39]. Therefore, VEGF increased gene expression could be caused by a direct binding between the VDR receptor and the VEGF promoter. Nevertheless this interaction remains to be tested.

3.5. 1α,25(OH)$_2$D$_3$ triggers apoptosis through Bim and p21 induction

Many studies have shown that A20 (ubiquitin editing enzyme A20 or *TNFAIP3*) functions as an "ubiquitin editing" enzyme to repress the signaling pathway of NF-κB, thus acting as a vital anti-inflammatory factor [40]. In addition, A20 expression has been found deregulated in several carcinomas and emerging evidence suggests that A20 participates in the development of cancer [41,42]. Particularly, in cells of hepatocarcinoma, it was demonstrated that A20 silencing causes cell death by apoptosis [42]. Besides, results from our group indicate that 1α,25(OH)$_2$D$_3$ induces apoptosis in vGPCR cells by increasing pro-apoptotic Bim protein; provoking an imbalance between the anti and pro-apoptotic proteins that ends

up into caspase-3 cleavage [26]. For this reason, we investigated whether 1α,25(OH)$_2$D$_3$ regulates A20 and Bim mRNA levels in MCS in dose response studies. To that end, vGPCR MCS were treated with 1α,25(OH)$_2$D$_3$ (0.1-100 nM) or vehicle (0.01% ethanol) during 48 hours and then mRNA expression of A20 and Bim was analyzed by qRT- PCR. As shown in **Fig. 5**, 1α,25(OH)$_2$D$_3$ significantly increased Bim mRNA expression in a dose-dependent manner, whereas not significant effect was found on A20 mRNA expression.

Numerous data have demonstrated that activation of cyclin-dependent kinase (CDK) inhibitors p18, p19, p21, or p27 and repression of cyclin D1 expression as well as down-regulation of cyclins/CDK complexes activity are early events for the growth-inhibitory effect of 1α,25(OH)$_2$D$_3$. For this reason, we investigated a possible regulation of p21 expression and contribution to apoptosis induction in vGPCR MCS. For this, vGPCR MCS were treated as in **Fig. 5** (**A** and **B)** and p21 mRNA expression was analyzed by qRT-PCR. As **Fig. 5 C** evidence, p21 mRNA expression was found increased by 1α,25(OH)$_2$D$_3$ in a dose dependent manner.

3.6. Akt and ERK1/2 phosphorylation is inhibited by 1α,25(OH)$_2$D$_3$

Akt plays a central role in the development of Kaposi's sarcoma produced by the transgenic expression of vGPCR; overexpression of vGPCR in endothelial cells inhibits apoptosis [43]. In addition, the effects of vGPCR on survival and angiogenesis depend on its ability to stimulate the MAPK pathway and, therefore, the transcription factors regulated by these kinases [44]. In this regard, ERK1/2 is highly activated in vGPCR cells [2]. Next, we investigated whether 1α,25(OH)$_2$D$_3$ regulates the state of Akt and ERK1/2 phosphorylation as part of its antineoplastic mechanism of action. For this purpose, dose response studies were performed as mentioned before. After treatment, vGPCR MCS were lysed in buffer and total proteins were resolved in SDS-PAGE followed by Western blot assays to identify phosphorylated Akt and ERK1/2, as an activation parameter. As shown in **Fig. 6**,

$1\alpha,25(OH)_2D_3$ causes a significant decrease in Akt and ERK1/2 phosphorylation in a dose dependent fashion.

4. Discussion

In many research laboratories, spheroids are becoming more and more used for the analysis of different pharmaceutical molecules and therapeutic agents. Their capacity to imitate several human tissues characteristics, as cellular organization, cell-cell and cell-extracellular matrix interactions, has made of 3D spheroids a highly demanded tool more appropriate as an *in vitro* model to represent solid tumors features [19,45,46]. There is data of various successful techniques to obtain spheroids [20,21,23]. Up to now, we have developed a simple method to obtain MCS from vGPCR endothelial cells. Our results provide compelling evidence that the viral receptor GPCR expression is vital for cells aggregation and MCS formation, since vGPCR absence showed a fast cell grouping with no size increase through time. The VDR high basal expression observed previously in vGPCR 2D cultures was verified in vGPCR MCS, demonstrating a similar behavior of the vitamin D receptor in this 3D model. $1\alpha,25(OH)_2D_3$ treatment disassembled vGPCR MCS morphology, raised VDR gene expression and inhibited HIF-1α contributing to the antiangiogenic effect. Although A20 showed no variations, gene expression of the pro-apoptotic protein Bim and of the cyclin-dependent kinase p21 were higher after $1\alpha,25(OH)_2D_3$ treatment, presenting the antineoplastic effect through an apoptotic mechanism of action. What is more, Akt and ERK1/2 signaling pathways, which play a central role in vGPCR oncogenesis, were inhibited by a reduced phosphorylated state in a dose dependent manner after treatment.

5. Conclusions

Taken together, most MCS data lends to support our previous results in vGPCR 2D cultures. Even though $1\alpha,25(OH)_2D_3$ performs antineoplastic and anti-angiogenic activity in vGPCR 2D and 3D cultures, these promising findings should be explore more deeply.

6. Acknowledgements

This work was supported by grants from Agencia Nacional de Promoción Científica y Tecnológica (ANPCYT, PICT 2013-0562), Consejo Nacional de Investigaciones Científicas y Tecnológicas (CONICET, PIP1122011010040), Universidad Nacional del Sur (PGI 24/B188) to Verónica González Pardo. The authors declare no competing or financial interests.

7. References

[1] E.A. Mesri, M. Feitelson, K. Munger, Human Viral Oncogenesis: A Cancer Hallmarks Analysis, Cell Host Microbe. 6 (2013) 266–282. doi:10.1021/nn300902w.Release.

[2] D. Martin, J.S. Gutkind, Kaposi's sarcoma virally encoded, G-protein-coupled receptor: a paradigm for paracrine transformation., Methods Enzymol. 460 (2009) 125–50. doi:10.1016/S0076-6879(09)05206-9.

[3] E.A. Mesri, E. Cesarman, C. Boshoff, Kaposi's sarcoma and its associated herpesvirus, Nat. Rev. Cancer. 10 (2010) 707–719. doi:10.1038/nrc2888.

[4] S. Montaner, A. Sodhi, A.K. Ramsdell, D. Martin, J. Hu, E.T. Sawai, J.S. Gutkind, The Kaposi's sarcoma-associated herpesvirus G protein-coupled receptor as a therapeutic target for the treatment of Kaposi's sarcoma, Cancer Res. 66 (2006) 168–174. doi:10.1158/0008-5472.CAN-05-1026.

[5] S. Montaner, A. Sodhi, A. Molinolo, T.H. Bugge, E.T. Sawai, Y. He, Y. Li, P.E. Ray, J.S. Gutkind, Endothelial infection with KSHV genes in vivo reveals that vGPCR initiates Kaposi's sarcomagenesis and can promote the tumorigenic potential of viral latent genes., Cancer Cell. 3 (2003) 23–36. doi:10.1016/S1535-6108(02)00237-4.

[6] F. Cheng, P. Pekkonen, S. Laurinavicius, N. Sugiyama, S. Henderson, T. Günther, V. Rantanen, E. Kaivanto, M. Aavikko, G. Sarek, S. Hautaniemi, P. Biberfeld, L. Aaltonen, A. Grundhoff, C. Boshoff, K. Alitalo, K. Lehti, P.M. Ojala, KSHV-initiated notch activation leads to membrane-type-1 matrix metalloproteinase-dependent lymphatic endothelial-to-mesenchymal transition, Cell Host Microbe. 10 (2011) 577–590. doi:10.1016/j.chom.2011.10.011.

[7] A. V Krishnan, D.L. Trump, C.S. Johnson, D. Feldman, The role of vitamin D in cancer prevention and treatment, Endocrinol.Metab Clin.North Am. 39 (2010) 401–18, table. doi:10.2174/18715281113129990046.

[8] A. V. Krishnan, D. Feldman, Mechanisms of the anti-cancer and anti-inflammatory actions of vitamin D., Annu. Rev. Pharmacol. Toxicol. 51 (2011) 311–36. doi:10.1146/annurev-pharmtox-010510-100611.

[9] J. García-Quiroz, R. García-Becerra, N. Santos-Martínez, D. Barrera, D. Ordaz-Rosado, E. Avila, A. Halhali, O. Villanueva, M.J. Ibarra-Sánchez, J. Esparza-López, A. Gamboa-Domínguez, J. Camacho, F. Larrea, L. Díaz, In vivo dual targeting of the oncogenic ether-à-go-go-1 potassium channel by calcitriol and astemizole results in enhanced antineoplastic effects in breast tumors, BMC Cancer. 14 (2014) 1–10. doi:10.1186/1471-2407-14-745.

[10] K.K. Deeb, D.L. Trump, C.S. Johnson, Vitamin D signalling pathways in cancer: Potential for anticancer therapeutics, Nat. Rev. Cancer. 7 (2007) 684–700. doi:10.1038/nrc2196.

[11] J. WELSH, Vitamin D and prevention of breast cancer, Acta Pharmacol. Sin. 28 (2007) 1373–1382. doi:10.1111/j.1745-7254.2007.00700.x.

[12] D.J. Mantell, P.E. Owens, N.J. Bundred, E.B. Mawer, A.E. Canfield, 1 ␣ ,25-Dihydroxyvitamin D 3 Inhibits Angiogenesis In Vitro and In Vivo, Growth Factors.

(2000) 214–220.

[13] M. Ben-Shoshan, S. Amir, D.T. Dang, L.H. Dang, Y. Weisman, N.J. Mabjeesh, 1 ,25-dihydroxyvitamin D3 (Calcitriol) inhibits hypoxia-inducible factor-1/vascular endothelial growth factor pathway in human cancer cells, Mol. Cancer Ther. 6 (2007) 1433–1439. doi:10.1158/1535-7163.MCT-06-0677.

[14] M.J. Larriba, N. Valle, H.G. Pálmer, P. Ordóñez-Morán, S. Alvarez-Díaz, K.-F. Becker, C. Gamallo, A.G. de Herreros, J.M. González-Sancho, A. Muñoz, The inhibition of Wnt/beta-catenin signalling by 1alpha,25-dihydroxyvitamin D3 is abrogated by Snail1 in human colon cancer cells., Endocr. Relat. Cancer. 14 (2007) 141–51. doi:10.1677/ERC-06-0028.

[15] H.G. Pálmer, J.M. González-Sancho, J. Espada, M.T. Berciano, I. Puig, J. Baulida, M. Quintanilla, A. Cano, A.G. de Herreros, M. Lafarga, A. Muñoz, Vitamin D(3) promotes the differentiation of colon carcinoma cells by the induction of E-cadherin and the inhibition of beta-catenin signaling., J. Cell Biol. 154 (2001) 369–87. doi:10.1083/jcb.200102028.

[16] D. Feldman, A. V. Krishnan, S. Swami, E. Giovannucci, B.J. Feldman, The role of vitamin D in reducing cancer risk and progression, Nat. Rev. Cancer. 14 (2014) 342–357. doi:10.1038/nrc3691.

[17] X. Cui, Y. Hartanto, H. Zhang, Advances in multicellular spheroids formation, J. R. Soc. Interface. 14 (2017). doi:10.1098/rsif.2016.0877.

[18] C.E. Rodríguez, S.I. Reidel, E.D.B. De Kier Joffé, M.A. Jasnis, G.L. Fiszman, Autophagy protects from trastuzumab-induced cytotoxicity in HER2 overexpressing breast tumor spheroids, PLoS One. 10 (2015) 1–16. doi:10.1371/journal.pone.0137920.

[19] G. Andrei, Three-dimensional culture models for human viral diseases and antiviral

drug development, Antiviral Res. 71 (2006) 96–107. doi:10.1016/j.antiviral.2006.05.023.

[20] E.C. Costa, A.F. Moreira, D. de Melo-Diogo, V.M. Gaspar, M.P. Carvalho, I.J. Correia, 3D tumor spheroids: an overview on the tools and techniques used for their analysis, Biotechnol. Adv. 34 (2016) 1427–1441. doi:10.1016/j.biotechadv.2016.11.002.

[21] E.C. Costa, D. de Melo-Diogo, A.F. Moreira, M.P. Carvalho, I.J. Correia, Spheroids Formation on Non-Adhesive Surfaces by Liquid Overlay Technique: Considerations and Practical Approaches., Biotechnol. J. (2017) 1–25. doi:https://doi.org/10.1002/biot.201700417.

[22] X. Xu, L.A. Gurski, C. Zhang, D.A. Harrington, M.C. Farach-Carson, X. Jia, Recreating the Tumor Microenvironment in a Bilayer, Hyaluronic Acid Hydrogel Construct for the Growth of Prostate Cancer Spheroids, Biomaterials. 6 (2013) 9049–9060. doi:https://doi.org/10.1016/j.biomaterials.2012.08.061.

[23] S. Shin, M. Ikram, F. Subhan, H.Y. Kang, Y. Lim, R. Lee, S. Jin, Y.H. Jeong, J.Y. Kwak, Y.J. Na, S. Yoon, Alginate-marine collagen-agarose composite hydrogels as matrices for biomimetic 3D cell spheroid formation, RSC Adv. 6 (2016) 46952–46965. doi:10.1039/c6ra01937d.

[24] V. González Pardo, A. Suares, A. Verstuyf, P. De Clercq, R. Boland, A.R. de Boland, Cell cycle arrest and apoptosis induced by 1α,25(OH)2D3 and TX 527 in Kaposi sarcoma is VDR dependent., J. Steroid Biochem. Mol. Biol. 144 Pt A (2014) 197–200. doi:10.1016/j.jsbmb.2013.11.014.

[25] V. González Pardo, N. D'Elia, A. Verstuyf, R. Boland, A. Russo de Boland, NFκB pathway is down-regulated by 1α,25(OH)(2)-vitamin D(3) in endothelial cells transformed by Kaposi sarcoma-associated herpes virus G protein coupled receptor.,

Steroids. 77 (2012) 1025–32. doi:10.1016/j.steroids.2012.05.006.

[26] A. Suares, A. Russo De Boland, A. Verstuyf, R. Boland, V. González Pardo, The proapoptotic protein Bim is up regulated by 1α,25-dihydroxyvitamin D<inf>3</inf> and its receptor agonist in endothelial cells and transformed by viral GPCR associated to Kaposi sarcoma, Steroids. 102 (2015) 85–91. doi:10.1016/j.steroids.2015.08.005.

[27] V. Gonzalez-Pardo, D. Martin, J.S. Gutkind, A. Verstuyf, R. Bouillon, A.R. de Boland, R.L. Boland, 1α,25-Dihydroxyvitamin D 3 and Its TX527 Analog Inhibit the Growth of Endothelial Cells Transformed by Kaposi Sarcoma-Associated Herpes Virus G Protein-Coupled Receptor in Vitro and in Vivo, Endocrinology. 151 (2010) 23–31. doi:10.1210/en.2009-0650.

[28] V. González Pardo, A. Russo de Boland, Age-related changes in the response of intestinal cells to 1α,25(OH)2-vitamin D3., Ageing Res. Rev. 12 (2013) 76–89. doi:10.1016/j.arr.2012.06.001.

[29] V. González Pardo, A. Verstuyf, R. Boland, A. Russo de Boland, Vitamin D analogue TX 527 down-regulates the NF-κB pathway and controls the proliferation of endothelial cells transformed by Kaposi sarcoma herpesvirus., Br. J. Pharmacol. 169 (2013) 1635–45. doi:10.1111/bph.12219.

[30] V. González Pardo, R. Boland, A.R. de Boland, 1alpha,25(OH)(2)-Vitamin D(3) stimulates intestinal cell p38 MAPK activity and increases c-Fos expression., Int. J. Biochem. Cell Biol. 38 (2006) 1181–90. doi:10.1016/j.biocel.2005.12.018.

[31] D. Martin, R. Galisteo, J.S. Gutkind, CXCL8/IL8 stimulates vascular endothelial growth factor (VEGF) expression and the autocrine activation of VEGFR2 in endothelial cells by activating NFκB through the CBM (Carma3/Bcl10/Malt1) complex, J. Biol. Chem. 284 (2009) 6038–6042. doi:10.1074/jbc.C800207200.

[32] A. Suares, M. Mori Sequeiros Garcia, C. Paz, V. González Pardo, Antiproliferative

effects of Bortezomib in endothelial cells transformed by viral G protein-coupled receptor associated to Kaposi's sarcoma., Cell. Signal. 32 (2017) 124–132. doi:10.1016/j.cellsig.2017.01.025.

[33] D. Martin, J.S. Gutkind, Human tumor-associated viruses and new insights into the molecular mechanisms of cancer, Oncogene. 27 (2008) S31–S42. doi:10.1038/onc.2009.351.

[34] E.A. Mesri, L.E. Cavallin, B.M. Ashlock, H.J. Leung, Q. Ma, P.J. Goldschmidt-Clermont, Molecular studies and therapeutic targeting of Kaposi's sarcoma herpesvirus (KSHV/HHV-8) oncogenesis, Immunol. Res. 57 (2013) 159–165. doi:10.1007/s12026-013-8458-z.

[35] S. Sakamoto, A.J. Ryan, N. Kyprianou, Targeting vasculature in urologic tumors: Mechanistic and therapeutic significance, J. Cell. Biochem. 103 (2008) 691–708. doi:10.1002/jcb.21442.

[36] R. Fukuda, B. Kelly, G.L. Semenza, Vascular Endothelial Growth Factor Gene Expression in Colon Cancer Cells Exposed to Prostaglandin E(2) Is Mediated by Hypoxia-inducible Factor 1, Cancer Res. 63 (2003) 2330–2334.

[37] A. Giaccia, B.G. Siim, R.S. Johnson, HIF-1 as a target for drug development, Nat. Rev. Drug Discov. 2 (2003) 803–811. doi:10.1038/nrd1199.

[38] G. A J, R. EB, NIH Public Access, Cell Death Differ. 15 (2014) 1–23. doi:10.1088/1367-2630/15/1/015008.Fluid.

[39] A. Cardus, S. Panizo, M. Encinas, X. Dolcet, C. Gallego, M. Aldea, E. Fernandez, J.M. Valdivielso, 1,25-Dihydroxyvitamin D3regulates VEGF production through a vitamin D response element in the VEGF promoter, Atherosclerosis. 204 (2009) 85–89. doi:10.1016/j.atherosclerosis.2008.08.020.

[40] S.G. Hymowitz, I.E. Wertz, A20: From ubiquitin editing to tumour suppression, Nat.

Rev. Cancer. 10 (2010) 332–340. doi:10.1038/nrc2775.

[41] B. Dong, G. Lv, Q. Wang, G. Wang, Targeting A20 enhances TRAIL-induced apoptosis in hepatocellular carcinoma cells, Biochem. Biophys. Res. Commun. 418 (2012) 433–438. doi:10.1016/j.bbrc.2012.01.056.

[42] L. Yin, Z. Fang, N.J. Shen, Y.H. Qiu, A.J. Li, Y.J. Zhang, Downregulation of A20 increases the cytotoxicity of IFN-γ in hepatocellular carcinoma cells, Drug Des. Devel. Ther. 11 (2017) 2841–2850. doi:10.2147/DDDT.S135993.

[43] A. Sodhi, S. Montaner, V. Patel, J.J. Gómez-Román, Y. Li, E.A. Sausville, E.T. Sawai, J.S. Gutkind, Akt plays a central role in sarcomagenesis induced by Kaposi's sarcoma herpesvirus-encoded G protein-coupled receptor., Proc. Natl. Acad. Sci. U. S. A. 101 (2004) 4821–6. doi:10.1073/pnas.0400835101.

[44] A. Sodhi, S. Montaner, J.S. Gutkind, Viral hijacking of G-protein-coupled-receptor signalling networks, Nat. Rev. Mol. Cell Biol. 5 (2004) 998–1012. doi:10.1038/nrm1529.

[45] H.S. Shin, Y.M. Kook, H.J. Hong, Y.M. Kim, W.G. Koh, J.Y. Lim, Functional spheroid organization of human salivary gland cells cultured on hydrogel-micropatterned nanofibrous microwells, Acta Biomater. 45 (2016) 121–132. doi:10.1016/j.actbio.2016.08.058.

[46] X. Xiang, Y. Phung, M. Feng, K. Nagashima, J. Zhang, V. Courtney Broaddus, R. Hassan, D. FitzGerald, M. Ho, The development and characterization of a human mesothelioma in Vitro 3D model to investigate immunotoxin therapy, PLoS One. 6 (2011) 1–10. doi:10.1371/journal.pone.0014640.

8. Figure Legends

Fig. 1. MCS development from SVEC and vGPCR cell lines. SVEC and vGPCR cells were seeded at a density of 2,500 cell/well in 96-well lipidure®-coat plates in triplicate and cultured in DMEM with 10 and 5% FBS respectively. Spheroids development was followed during a seven days period. Micrographs shown are representative from three independent cultures. Magnification 200 x, bar =100 µm.

Fig. 2. vGPCR and VDR gene expression in vGPCR MCS. Total RNA from Spheroids at 5th day-growth (Fig.1) was extracted and reverse transcribed as described in methods. Gene expression of vGPCR, VDR and GAPDH was assessed by qRT-PCR analysis. Data were expressed in bar graphs as a ratio between each gene expression from SVEC and vGPCR spheroids normalized to GAPDH mRNA levels.

Fig. 3. 1α,25(OH)$_2$D$_3$ induces morphological changes and increases VDR expression in vGPCR MCS. vGPCR cells were seeded at a density of 2,500 cell/well in 96-well lipidure®-coat plates and cultured in DMEM with 5% FBS. At 5th day-growth, spheroids were treated with increasing concentrations of 1α,25(OH)$_2$D$_3$ (10-100 nM) or vehicle (0.01% ethanol) for 48 hours. (**A**) Representative micrographs from three independent experiments are shown; magnification 200 x, bar =100 µm. (**B**) Gene expression of VDR and GAPDH was assessed by qRT-PCR analysis as was mentioned in methods. Results from VDR expression were then represented in a bar graph as a ratio between treated conditions and vehicle normalized to GAPDH mRNA levels. The statistical significance of the data was analyzed by one way-ANOVA followed by Bonferroni test. Different letters indicate statistical differences (*$p<0.05$), n=6.

Fig. 4. 1α,25(OH)$_2$D$_3$ reduces HIF-1α and induces VEGF gene expression. vGPCR MCS were developed, grown and treated as in **Fig. 3**. Gene expression of HIF-1α, VEGF and GAPDH was assessed by qRT-PCR analysis as was described in methods. Results

from each gene analysis were represented in bar graphs expressing the ratio between treated conditions and vehicle normalized to GAPDH mRNA levels. The statistical significance of the data was analyzed by one way-ANOVA followed by Bonferroni test. Different letters indicate statistical differences (*p<0.05), n=6.

Fig. 5. 1α,25(OH)$_2$D$_3$ promotes Bim and p21 induction. vGPCR MCS were developed, grown and treated as in Fig. 3. Gene expression of A20, Bim, p21 and GAPDH was assessed by qRT-PCR analysis as was described in methods. Data from each gene expression were expressed in bar graphs as a ratio between treated conditions and vehicle normalized to GAPDH mRNA levels. Significant differences of the data between vehicle and treated conditions were analyzed by one way-ANOVA followed by Bonferroni test. Different letters indicate statistical significances at *p<0.05, n=6.

Fig. 6. 1α,25(OH)$_2$D$_3$ reduces Akt and ERK 1/2 phosforylated state. vGPCR MCS were developed, grown and treated as in Fig. 3. Cell lysates were subject to Western blot analysis with anti-P-Akt, anti-P-ERK 1/2 and anti-Tubulin antibodies. Representatives blots and quantifications of three independent experiments are shown. Protein bands quantification were achieved by densitometry and then represented in bar graphs as the ratio between P-ERK1/2 and Tubulin, and P-Akt and Tubulin referred to vehicle. Four independent experiments were analyzed by one way-ANOVA followed by Bonferroni test. Different letters indicate statistical significances at *p<0.05.

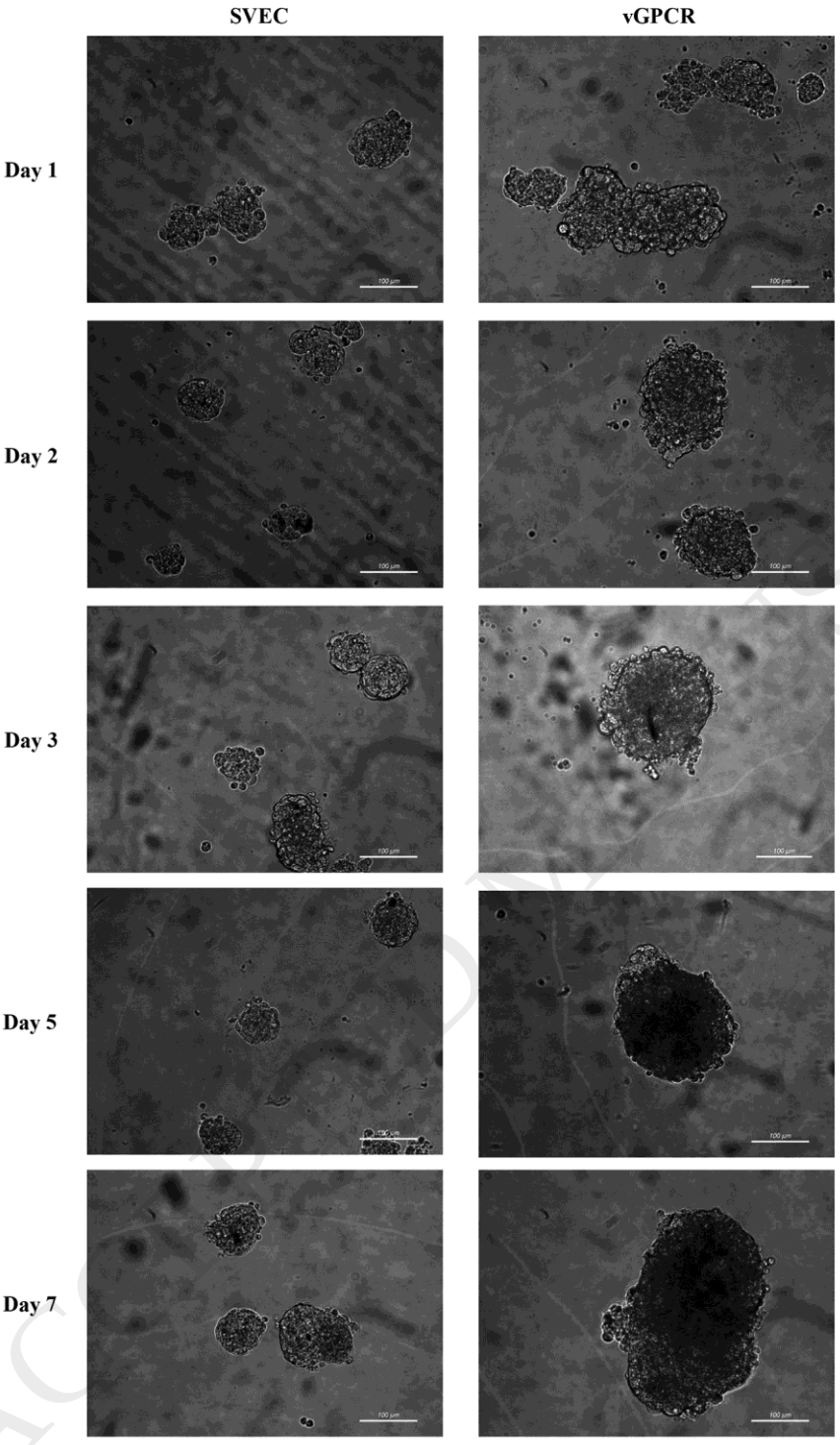

Fig. 1

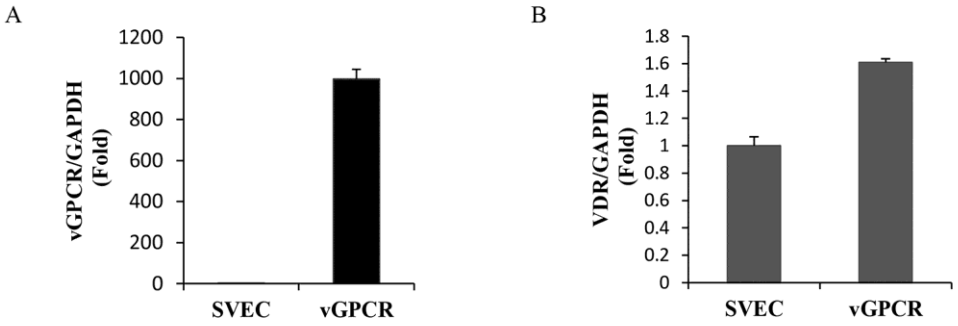

Fig. 2

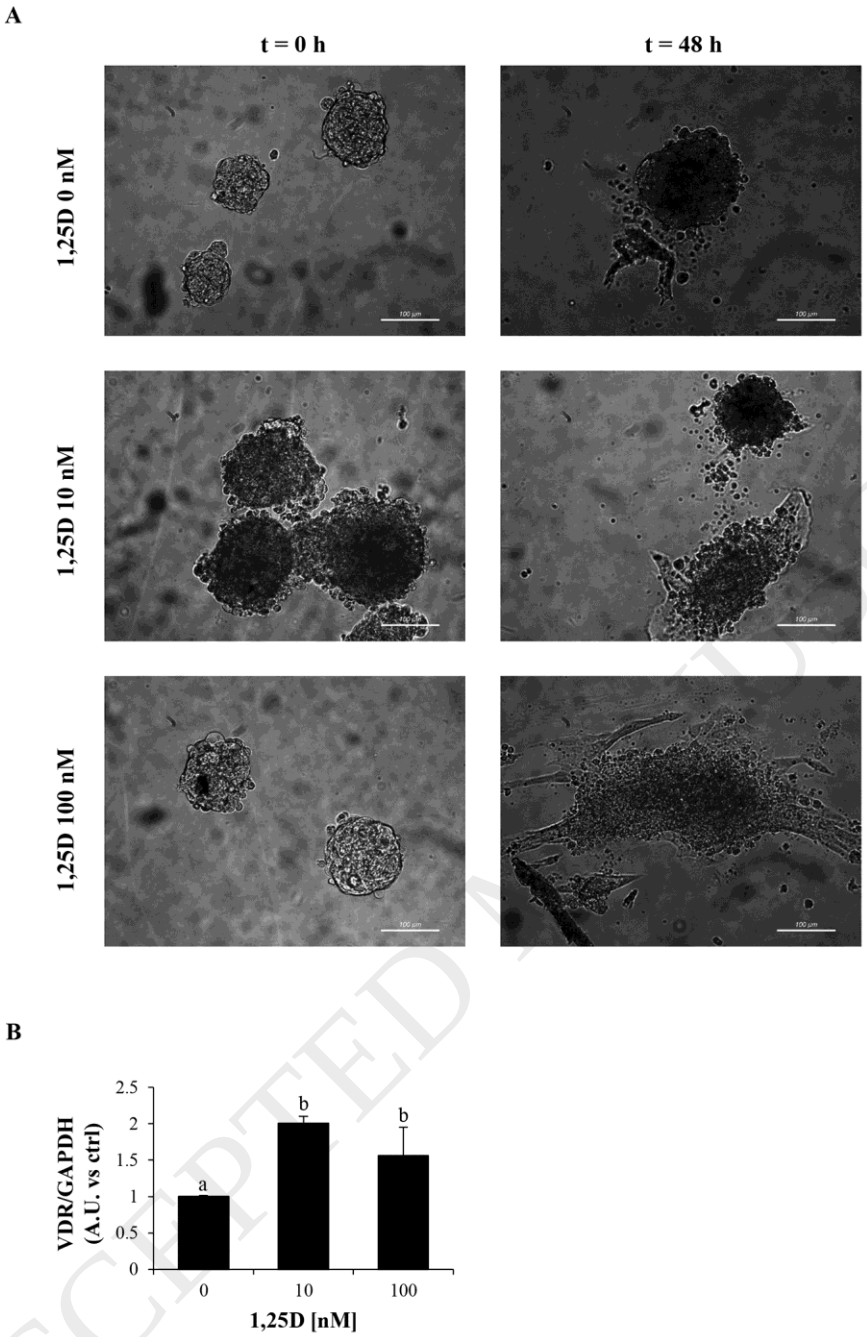

Fig. 3

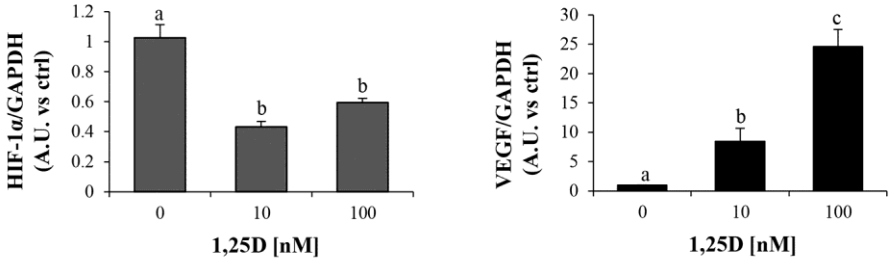

Fig. 4

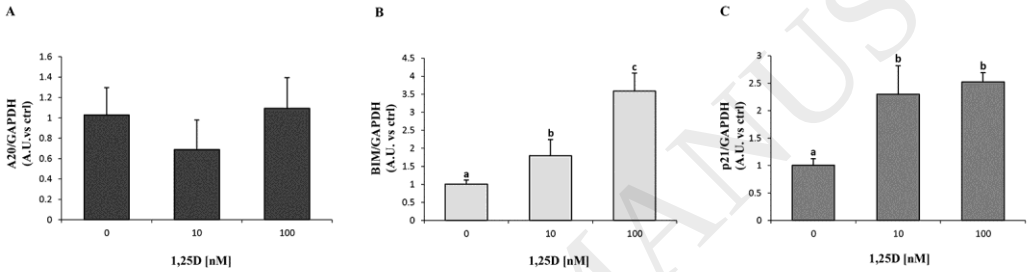

Fig. 5

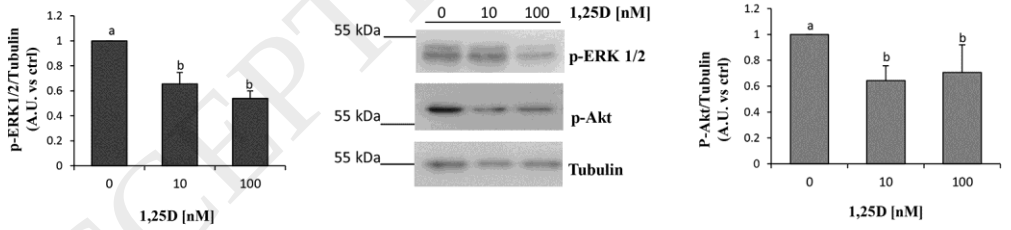

Fig. 6